THE JOURNAL OF PHYSICAL CHEMISTRY B

ARTICLE

pubs.acs.org/JPCB

Tracking of the Polyproline Folding by Density Functional Computations and Raman Optical Activity Spectra

Václav Profant,[†] Vladimír Baumruk,[†] Xiaojun Li,[‡] Martin Šafařík,[§] and Petr Bouř*[,§]

[†]Faculty of Mathematics and Physics, Charles University, Ke Karlovu 5, 12116, Prague 2, Czech Republic

[‡]Department of Chemistry, Centre for Theoretical and Computational Chemistry, University of Tromsø, N-9037 Tromsø, Norway

[§]Institute of Organic Chemistry and Biochemistry, Academy of Sciences, Flemingovo nám. 2, 166 10 Prague, Czech Republic

Supporting Information

ABSTRACT: Polyprolines offer many opportunities to study factors influencing peptide and protein folding and structure. Longer chains can adopt two well-defined forms (PPI and PPII), but shorter peptides are quite flexible. To understand in detail the dependence of the secondary structure on the length and the interplay between the side chain and main chain conformation, zwitterionic $(Pro)_N$ models (with N = 2, 3, 4, 6, 9, 12 and longer inhomogeneous chains) were studied by a combination of the Raman and Raman optical activity (ROA) spectroscopy with the density functional theory (DFT). Potential surfaces were systematically explored for the shorter oligoprolines, and Boltzmann conformational ratios were obtained both for the main chain and the proline ring puckering. The predictions were verified by comparison of the experimental and simulated ROA spectra. The conformer ratios extracted from a decomposition of the experimental ROA into scaled computed spectra well reproduced Boltzmann populations calculated from relative energies. For example, an "A" puckering of the proline ring was found prevalent, relatively independent of the length, whereas the *cis*-amide backbone form adopted by shorter peptides rapidly disappeared for $N > 4$. The results are consistent with previous NMR and vibrational circular dichroism (VCD) data. Delocalized exciton vibrations along the peptide chain often enhance the ROA signal, and can thus be used to indicate a longer regular peptide structure. The ROA technique appeared to be very sensitive to the ring puckering; less distinct spectral features were produced by changes in the main chain geometry.

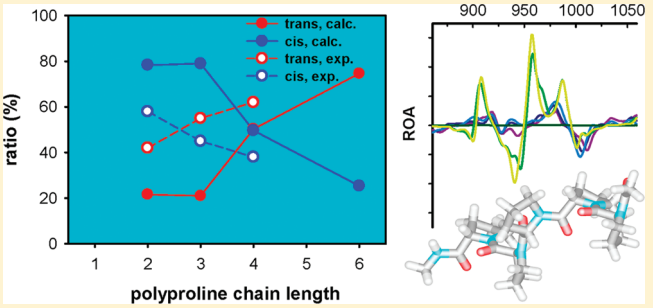

INTRODUCTION

Conformational behavior of the proline residue attracts attention because of its unique properties. Unlike for the other genetically coded amino acids, prolines in a peptide chain are linked through imine residues. They cannot form intermolecular hydrogen bonds. However, the molecular structure is strongly stabilized by interaction with the solvent environment, mostly by the hydration sphere attached to the carbonyl groups. The hydrophobic interactions can also be very strong and were recently suggested to stabilize anion complexes.[1] Proline conformation is obviously strongly restricted by the five-membered ring. Unique properties of the proline residue are reflected also in peptides; for example, lone-standing proline residues in the peptide chains usually induce β-turns.[2−5]

Nowadays, a renewed interest for polyprolines is apparent in macromolecular chemistry, as these polymers appeared suitable for well-defined components of self-assembling aggregates.[6,7] The conformational properties can be finely tuned by chemical modification of the proline units.[8−11] For example, β-prolines were suggested as inhibitors of protein−protein recognition events.[12]

Polyproline systems have also been intensively studied for their unique folding properties and as canonical models of the "unordered" protein structure. In water, but also in organic acids or benzyl alcohol, the OR, CD, NMR, and vibrational circular dichroism (VCD) spectroscopies revealed that from certain chain length oligoproline adopts the typical "polyproline II" (PPII) left-handed helix.[13−15] This form is very close to the random coil secondary structure exhibited also by peptides, which do not contain the proline residue.[16−19] PPII helix was suggested to be involved in many processes, for example, in the denaturation mechanism of prion proteins.[20] The other regular conformation of polyproline, "polyproline I" (PPI), is a right-handed helix with *cis*-peptide bonds.[21] For longer oligoprolines, it may be obtained in more hydrophobic solvents, such as aliphatic alcohols or pyridine.[16]

The dependence of the oligoproline conformation on the peptide chain length investigated in the present study is another interesting aspect, intensively studied in the past.[22] However, interpretations of experiment were often inconclusive or provided conflicting messages. The transition between the PPI and

Received: August 11, 2011
Revised: October 10, 2011
Published: November 07, 2011

ACS Publications © 2011 American Chemical Society

PPII forms was soon recognized to be a complex cooperative process, dependent also on the solvent polarity.[22,23] The tetramer $(Pro)_4$ was suggested as a structure with minimal PPI content in methanol, but for other solvents and in other studies, a monotonic dependence was reported.[24] For shorter polymers, the conformation is strongly influenced by eventual protection of the terminal groups.[13,23,24] Proline dimer and the shortest polymers seem to exhibit the richest conformational freedom, quite difficult to study experimentally.[23,24]

Computational chemistry provided alternate insight into the correlations between oligoproline secondary structure, ring puckering, chain length, and solvent environment.[9,25] For example, a slight propensity to a "down" ring puckering was predicted, and a mixture of *cis*−*trans* (PPI−PPII) conformers was suggested based on vacuum computations, with a domination of the *trans*-form.[8,26,27] Several experimental and theoretical studies analyzed the interplay between side chain and main chain conformations.[28−32]

Understanding of the folding process is also important for proline optical rotatory dispersion (ORD) studies, where improper conformer averaging can even lead to wrong absolute configuration.[33] The Raman optical activity (ROA) appeared particularly sensitive to the side chain conformation, that is, to the five-member ring puckering.[34,35] Latest theoretical study on Ac-$(Pro)_n$-Me suggested that a rich conformer equilibrium exists even for considerably long peptides.[8,36,37] However, ab initio test on smaller systems sometimes provided significantly different conformer energies than empirical MD force fields.[38] Neither were some MD force fields accurate enough to reproduce NMR experiments on proline dipeptides.[28]

Taking advantage of the ROA spectroscopy and accurate DFT methods in this study allowed us to obtain a deeper insight into the folding process. For example, in previous NMR studies an average puckering is observable only, whereas the ROA spectroscopy, at least in principle, can detect individual conformers by an algebraic decomposition of measured spectrum.[34,39] We performed a systematic conformational search of shorter oligoprolines at the DFT level. At about these lengths (N = 2, ..., 12), the transition between the conventionally unordered and regular PPII structure takes place.[16,25] By comparison of calculated and experimental spectra, we could identify spectroscopic marker patterns associated with particular backbone or side chain features.

The calculated potential energy surfaces (PES) were not only able to consistently explain the oligoproline behavior observed in the previous experiments, but also provided observed progression of spectral intensities and revealed detailed conformer distributions of the backbone and the puckering. The analysis of computed parameters confirmed the previously proposed coupling of the side chain and the backbone. The polyproline I conformation of the backbone is stable only for the shortest (N < 3) structures, whereas for the longer one, polyproline II prevails. However, according to our results, regular polyproline segments are rather short and *cis*-residues occasionally occur even for long proline chains. The peptide folding with the increasing chain length appears as a gradual dynamic process.

Based on the conditions optimized in a previous study,[40] Raman and ROA spectra of NH_3^+-$(Pro)_N$-COO^- (N = 2, 3, 4, 6, 9, and 12), short ($N \sim 50$), medium ($N \sim 200$), and long (N > 300) polyprolines were recorded in aqueous solutions. The experimental spectra were compared to the simulated vibrational frequencies and intensities. The Boltzmann averaging of many conformers provided a faithful description of the experimental spectra and enabled to assign specific bands to the proline puckering and secondary structure. For the first time, excitone-like enhancement of the ROA/Raman circular intensity difference (CID) ratio of a regular peptide structure was observed, similarly as for DNA VCD.[41] The results thus confirm that the ROA spectroscopy can be used to monitor both local and longer-range structural features.

The ROA spectra comprise difference in scattering of the right and left circularly polarized light and are more sensitive to the conformation than normal Raman scattering. Both spectral kinds can easily be obtained within the physiological aqueous environment. The ROA technique was already applied to systems ranging from gas phase isolated molecules,[42] oversimple organic compounds,[43,44] peptides,[45−47] proteins,[48,49] nucleic acids,[50] to viruses.[48,51] Although it senses vibrational properties of whole molecules, it also provides a reasonably local probe of molecular sites.[46,52]

Previously, the vibrational optical activity techniques already gave important information about the geometry of proline residue[34,53] and longer proline polymers.[54,55] Vibrational frequencies were assigned to polyproline normal modes.[11] PPII chain length dependence was studied by the vibrational circular dichroism (VCD).[16,17,56] However, the VCD data focused primarily on the backbone conformation and could be interpreted on an empirical basis so far.

Today, interpretation of ROA is unthinkable without quantum computations. We conveniently employ the latest analytical derivative techniques that replaced previous tedious numerical differentiation of ROA tensors.[57−59] Coupled-perturbed DFT computations using the gauge independent atomic orbitals (GIAO)[60] enabled us to faithfully model spectroscopic properties of considerably long oligoproline chains at a high approximation level. For example, the spectra up to the nonamer could be calculated quantum mechanically. By the Cartesian coordinate tensor transfer technique (CCT),[61] the computation could be further extended to virtually unlimited chain lengths, under an acceptable loss of accuracy.[62,63] Simulated spectral features are in a very good agreement with the observations, and the computations also well reproduce the observed length dependence. The spectra also clearly show that a one-conformer model is adequate neither for shorter sequences, nor for longer polyprolines.

EXPERIMENTAL METHODS AND CALCULATIONS

Spectroscopic Experiments. The used Raman and ROA experimental procedures are described elsewhere in detail;[64] see also Table S1 in Supporting Information (SI). Commercial $(Pro)_N$ peptides were used for N = 2, 3, 4, and for the longest heterogeneous polyproline polymers with a medium molecular weight of 1000−10000 g/mol (short, "*S*", $N \sim$ 50), 10000−30000 g/mol (medium, "*M*", $N \sim 200$) and, >30000 g/mol (long, "*L*", N > 300). Sequences with N = 6, 9, and 12 were obtained by standard methods of peptide resin synthesis using the FMOC (9-fluorenylmethyloxycarbonyl) strategy. We used the unblocked peptides because of the good solubility required for the ROA spectroscopy. The zwitterionic molecules, not so much investigated in previous studies, are also perhaps more related to the biological importance than more usual protected peptides.

With our spectrometer,[65] backscattered Raman and ROA spectra were obtained for aqueous solutions at 293 K. Typical

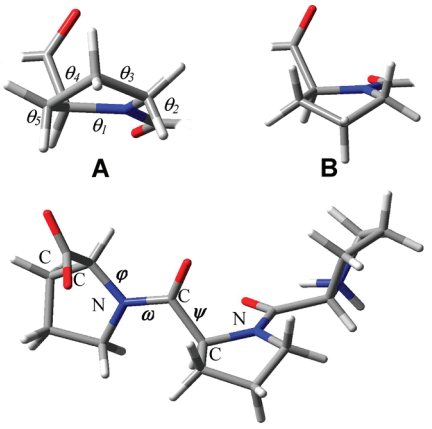

Figure 1. Definition of the two puckered proline ring conformers (A, B, according to ref 34), and the backbone torsion angles $\varphi = \angle(C,C,N,C)$, $\omega = \angle(C,N,C,C)$, $\psi = \angle(N,C,C,N)$. The puckering is defined by the phase P, $\tan(P) = (\theta_3 + \theta_5 - \theta_2 - \theta_4)/\{2\theta_i[\sin(\pi/5) + \sin(2\pi/5)\}$, and amplitude $\theta_m = \theta_1/\cos(P)$.[67]

laser power at the sample was 500 mW, concentration 0.4 M, and collection time of one spectrum 20 h. The experimental Raman spectra were normalized to the average intensities of peaks at 1100 and 1271 cm^{-1}. The corresponding ROA spectra were multiplied by the same normalization factor as the Raman signal. An alternate normalization based on integral intensities led to similar results; by default, we use the peak normalization procedure, as it is not influenced by traces of trifluoracetic acid (TFA) impurities that needed to be subtracted in limited wavenumber regions for the synthetic oligoprolines (N = 6, 9, and 12). The TFA signal is also subtracted in the presented Raman spectra.

Potential Energy Scans. The two A and B puckering types (see ref 34) and the backbone torsion angles φ, ψ, and ω are defined in Figure 1. The A and B types correspond to the "down" and "up" conformers also used in literature.[66] The proline ring conformation was also characterized by the usual pseudorotation phase P, $\tan(P) = (\theta_3 + \theta_5 - \theta_2 - \theta_4)/\{2\theta_i[\sin(\pi/5) + \sin(2\pi/5)\}$, and amplitude $\theta_m = \theta_1/\cos(P)$.[67] For the A conformer, $P \sim 110°$ and $\theta_m \sim 37°$; for B, $P \sim 280°$ and $\theta_m \sim 38°$.[34] Note that all these puckering definitions do not determine the ring geometry unambiguously and are used for a quick orientation only.

The φ angle is determined by the puckering, and the ψ angle can only adopt a value close to 160°. This was verified for the dimer, where four puckering types (AA, AB, BA, and BB) × 2 ω angle values (ω = 0 and 180°, corresponding to the *cis*- and *trans*-conformation of the amide bond) × 3 ψ angles (−80, 40, and 160°) generated 24 conformers. Conformers with ψ differing much from 160° were energetically strongly disfavored. For the trimer, we selected the A puckering to prescan the complete backbone potential energy surface, generating $2(\omega) \times 3(\psi) \times 2(\omega) \times 3(\psi) = 36$ conformers. As for the dimer, structures with ψ deviating from 160° appeared as quite unrealistic, with relative energies higher than 5 kcal/mol.

Putting the starting ψ angle at 160°, we generated trimer and tetramer conformer geometries differing in the puckering and the peptide bond ω angle, which provided 32 and 128 structures, respectively. For the hexamer, about 2048 conformers are possible. Their systematic investigation is currently beyond our computational capabilities (currently over 100 years of computer time would be needed for consistent optimization and spectral simulation, for Intel 3 GHz CPU). Fortunately, a limited number of 64 conformers could be preselected, as described below, based on the conformer patterns obtained for the shorter sequences.

Table 1. Calculated Relative Conformer Electronic Energies (kcal/mol) of the $(Pro)_2$ Dimer[a]

conformer	B3LYP[b]	B3LYP	B3LYP[c]	B3LYP[d]	B3LYP-D	BPW91
AcA	0.0	0.0	0.0	0.0	0.0	0.0
AcB	1.1	0.5	0.4	0.5	0.8	0.5
BcA	0.4	0.1	0.1	0.1	0.5	0.3
BcB	1.5	0.5	0.5	0.5	0.9	0.7
AtA	2.4	0.9	0.9	0.9	1.4	1.0
AtB	3.4	1.0	1.0	1.0	1.8	1.1
BtA	3.4	1.1	1.1	1.0	2.1	1.3
BtB	3.8	1.1	1.1	1.0	2.3	1.3

[a] By default, the 6-311++G** basis set was used with the CPCM(H_2O) solvent correction. [b] 6-31G**. [c] aug-cc-pVDZ. [d] aug-cc-pVTZ.

The Gaussian[68] program suite was used for the DFT computations. By default, the B3LYP[69] functional with the 6-311++G** basis set and the CPCM(H_2O)[70] solvent correction were used. The standard Gaussian UFF model[71] was used for the solvent radii. For eight lowest-energy conformers of the dimer, a wider range of the functionals (B3LYP, BPW91, and dispersion-corrected[72] B3LYP (D-B3LYP)) and basis sets (6-311++G**, 6-31G**, aug-cc-pVDZ, and aug-cc-pVTZ) was applied to estimate the reliability of the results. For the chains with N = 2, 3, 4, and 6, the 6-31++G** basis set was also applied, providing only minor changes if compared to the 6-311++G** results. Some conformers of oligoprolines with N = 9 and 12 were optimized at the B3LYP/CPCM(H_2O)/6-31G** level to verify the puckering preference, for the PPII main chain conformation only.

Raman and ROA Spectra Simulations. The Raman and ROA spectra were also computed by Gaussian at the same B3LYP/CPCM(H_2O)/6-311++G** level as for the equilibrium structures. Backscattered (180°) Raman and ROA spectral profiles were obtained from the intensities (I_{180}) calculated for the excitation laser light of 514.5 nm by a convolution with Lorentzian function and the Boltzmann correcting factor as

$$S(\omega) = I_{180}\left[1 - \exp\left(-\frac{\omega_i}{kT}\right)\right]^{-1}\frac{1}{\omega_i}\left[4\left(\frac{\omega - \omega_i}{\Delta}\right)^2 + 1\right]^{-1}$$

(where T = 273 K, k is the Boltzmann constant, ω_i is the vibrational frequency, and the bandwidth Δ = 10 cm^{-1}.

For longer peptides (N > 6), the Cartesian coordinate tensor transfer (CCT) technique[61] was used to generate the force field and optical activity tensors from smaller tetrameric fragments. The method is schematically depicted in Figure S1 in SI. The accuracy of this approach may be limited according to the chosen transfer scheme.[52,62,63,73] However, in our case, it produced reasonable approximation for the ROA signal at least in the higher-frequency range (>600 cm^{-1}, cf., Figure S2).

RESULTS AND DISCUSSION

Relative Conformer Energies. For the dimer, relative conformer energies for the eight lowest-energy conformers obtained at several approximation levels are listed in Table 1. Relevant geometric parameters calculated at the default B3LYP/CPCM-(H_2O)/6-311++G** level can be found in Table S2.

Table 2. Calculated (B3LYP/6-311++G/CPCM/H2O) Relative Conformer Electronic (ΔE), Zero Point (ZPE), Enthalpies (ΔH), and Free (ΔG) Energies (kcal/mol) of the $(Pro)_N$ Oligomers (N = 2, 3, 4, and 6); Boltzmann Populations η Are Based on ΔE + ZPE**

conformer	ΔE	ΔE + ZPE	ΔH	ΔG	η (%)
Dimer					
AcA	0.0	0.0	0.0	0.0	28
BcA	0.1	0.1	0.2	0.0	23
AcB	0.5	0.4	0.4	0.3	15
Trimer					
BcBcA	0.1	0.0	0.0	0.0	23
AcAcA	0.0	0.1	0.0	0.6	20
BcAcB	0.6	0.7	0.7	1.2	7
Tetramer					
BcAcAcA	0.0	0.0	0.3	0.2	7
AcAcAcA	0.6	0.1	0.0	2.3	6
AtAcAcA	0.6	0.2	0.7	0.0	5
Hexamer					
BtBtAtAtAtA	0.1	0.0	0.0	0.4	16
AtBtAtAtAtA	0.0	0.1	0.0	1.4	13
AtAtAtAtAtA	0.1	0.3	0.7	0.2	10

The AcA (abbreviated for AA puckering and *cis*-peptide bond between the two proline residues; similarly, we use "t" for the *trans*-peptide bond) conformer is predicted to have the lowest energy by all the methods (Table 1). For B3LYP, the 6-31G** basis set provides significantly different relative energies than the larger 6-311++G**, aug-cc-pVDZ and aug-cc-pVTZ basis sets. Because there are virtually no differences between 6-311++G** and supposedly more accurate aug-cc-pVTZ, we can consider the 6-311++G** basis to be a sufficient compromise with respect to the speed and accuracy also for the longer oligoprolines.

The Grimme empirical van der Waals correction[72] in the B3LYP-D method (6th column in Table 1) causes a significant change in the relative energy of the third conformer (0.1 → 0.5 kcal/mol); otherwise, it mostly conserves the trends predicted by plain B3LYP. Thus, the correction needed for van der Waals complexes[74] may not be so important for the prolines stabilized by electrostatic interactions. Neither the B3LYP-D model comprises the solvent−solute dispersion. Therefore, we use the uncorrected B3LYP functional as default. For trial computations, dispersion-corrected Boltzmann averages provided spectra very similar to the uncorrected ones. The dispersion influence on the dimer conformation was lately studied in detail in ref 75. The GGA BPW91 functional (last column) provides similar (within 0.2 kcal/mol) conformer energies as B3LYP. B3LYP, however, provides better overall spectral profiles than BPW91.[46,73,76,77]

In Table 2, computed electronic energies, zero point energies (ZPE), enthalpies, and Gibbs energies are listed for three lowest energy conformers of the dimer, trimer, tetramer, and hexamer oligoprolines. The ZPE correction has a relatively minor effect on the energies. Similarly, the enthalpies (ΔH) mostly follow the electronic energies, except for the tetramer, where the ordering of the two lowest-energy conformers is switched. The free (Gibbs, ΔG) energies deviate even more from ΔE. We consider the ΔE + ZPE sum or ΔH to yield the most realistic conformer distributions. The free energy obtained from Gaussian can be hampered by the simplifications used, in particular, by the harmonic approximation, rotational, and translational partition function for a solitary molecule, and neglect of the solvent.[78] Although the enthalpies and free energies sometimes provide different conformer ordering, after the Boltzmann averaging very similar spectra are obtained by both approximations. In general, the trends and magnitudes of the relative conformer energies (Table 2) are consistent with previous computations performed in vacuum or for blocked peptides.[8,26] However, for the zwitterionic molecules, we predict larger ratios of the *cis*-forms, probably because of the effect of the charged residues, whereas for longer peptides, the role of the termini is presumably minor; for shorter oligopeptides, they significantly influence the peptide conformation.[79,80]

Geometry and Peptide Folding. From the relative conformer energies (partially listed in Table 2), we deduce that the percentage of the *trans*-peptide bonds typical for the PPII conformation increases with the peptide chain length. Nevertheless, in tetramer the *cis*-conformation still dominates; for hexamer, all the three lowest-energy conformers are trans. In an adiabatic approximation the *cis*/*trans*-isomerization can be thought of as independent of the puckering. This can be documented on the dimer (Table 1), where the c ↔ t change is associated with a larger energy (~2 kcal/mol) than the A ↔ B inversion (<1 kcal/mol).

For the longer proline oligomers, however, the amide bond−proline ring interaction plays a significant role and leads to relatively complicated conformer ordering. The puckering B is generally preferred at the N-terminus, whereas A is accumulating at the C-end. For example, the predicted population of AAAAAB is 2.06%, and BBBBBA has 0.88% in the hexamer. The alternating AB arrangement adopts 20% in the trimer, 10% in tetramer, and 2.5% (1.1% of ABABAB + 1.4% of BABABA, whereas statistical probabilities are 1.5% = $1/2^6$) in the hexamer. The A puckering is in general preferred over B; in the hexamer, the AAAAAA form adopts 4.4% and pure BBBBBB 0.4%. For long all-*trans*-polyprolines ($(Pro)_N$ in PPII secondary structure), the computations suggest that the most probable puckering pattern is close to the "$B_{N/2}A_{N/2}$" formula, that is, the A puckering accumulates at the C-terminus.

As shown in Figure 2 (overview of the $\theta_m(P)$ dependence of the puckering coordinates) or Table S3 (selected coordinates for hexamer conformers), the detailed puckering geometry somewhat depends on the position in the oligoproline chain. The terminal residues differ from the inner ones. In particular, the N-terminus is more puckered ($\theta_m \sim 40°$) than the inner and C-terminal rings, where $\theta_m \sim 37°$ (Table S3).

The computed main chain (ω, φ, and ψ) angles (e.g., Table S3) correspond well with the standard polyproline I (0°, −83°, 158°, 3.1 Å translation per residue) and II (180°, −78°, 149°, 1.9 Å translation per residue) parameters obtained by X-ray.[81] The angle ω occasionally deviates from the planar arrangement, by up to 5°, due to the flexibility of the amide bond.[82] For the *trans*-conformers, the φ and ψ angles are notably different for the B ($\varphi \sim -62°$, $\psi \sim 146°$) and A ($\varphi \sim -75°$, $\psi \sim 159°$) puckering.

To investigate more the relation between the ring puckering and main chain PPII angles, we analyzed B3LYP/CPCM/6-311++G** equilibrium geometries of the proline hexamer, with all puckering patterns (64 different conformers). As can be seen in Figure 3, correlations between the secondary structure and the puckering coordinates exist, which in general also explains the

complicated conformational ordering (nonadditivity of the backbone and side chain conformer energies) discussed above. The φ angle is part of the ring and is well correlated with the phase θ_m and amplitude P within the two puckering groups. Rather surprisingly, there is also some correlation between the puckering coordinates and the ψ and ω angles not directly involving the ring. The A puckering type (with the phase $P \sim 100°$, right-hand side of Figure 3) clearly enforces smaller φ-angles ($\sim -75°$) than the B-type, where $\varphi \sim -63°$. For ψ, the values around 159 and 146° are most typical for the A and B puckering, respectively.

The angle ω weakly correlates both with the phase and the amplitude. For the B puckering, the ω-distribution is significantly wider (172−180°) than for A (177−180°). The distribution is primarily caused by the position of the residue in the hexamer; for example, the peptide bond is more planar ($\omega \sim 180°$) around the N-terminus than close to the C-terminus ($\omega \sim 175°$). We find the dependence of the secondary structure on the side chain conformation interesting, as it may be important in protein folding and structural applications. For an A-puckered ring in *trans*-polyproline, for example, the translation distance per residue is significantly larger than for the B-puckering. The results are in agreement with previous experimental observations,[29] where the φ main chain angle was slightly more correlated with the puckering than with the ψ angle.

Similar analysis was done for the correlation between the ω angle (cis, trans) and the main chain ψ and φ angles, for all A-puckered conformers. *cis*-Peptides exhibited distinct values of $\psi \sim 162°$ and $\varphi \sim -80°$, while for trans $\psi \sim 158°$ and $\varphi \sim -75°$. However, terminal residues differed. Additionally, weaker correlations were predicted at the N-end.

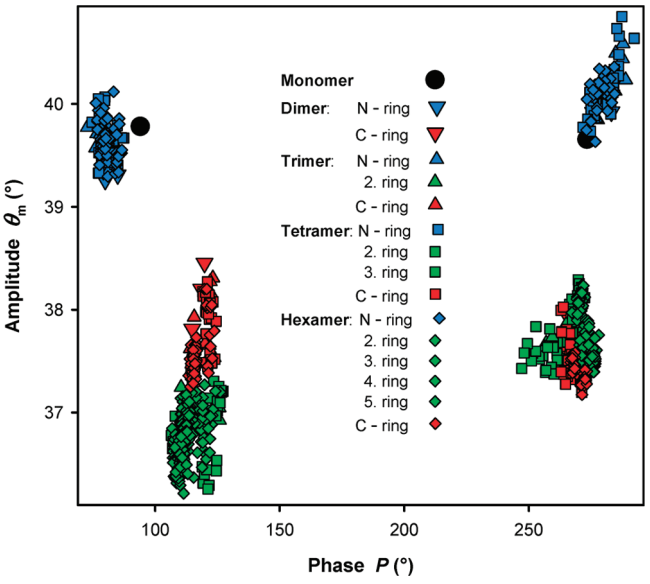

Figure 2. Dispersion of the two puckering coordinates, amplitude θ_m, and phase P (cf. Figure 1 for definition) in the equilibrium conformers of $(Pro)_N$.

Raman and ROA Spectral Length Dependence. As documented in Figure 4 with the experimental spectra, the many Raman and ROA bands exhibit a consistent progression with the peptide chain length if normalized to the dominant peaks. The good baseline stability and the low noise level allow us to compare the spectral changes (details summarized in Table S4) to the simulations. The vibrational assignment (Table S4) agrees with the discussion of the ROA features in ref 35 and other works.[11] In Figure 4 we can see that, for example, the C═O stretching ROA and Raman intensities (around 1620 cm^{-1}) increase quickly with N, until $N \sim 12$. For $N = 2$ Raman signals of the terminal COO^- carbonyl stretching (1570 cm^{-1}) and terminal NH_2^+ bending (1401 cm^{-1}) are clearly apparent; these, however, gradually disappear for longer chains. Very clear are also build-ups of the ROA intensity at 325, 405, 535, 946, 978, 999, 1195, and 1208 cm^{-1}; typically the Raman signal is rather constant, so that the CID (ROA/Raman circular intensity ratio) increases with N. On the other hand, the Raman signal around 510 cm^{-1} becomes relatively very strong for a longer chain, but it is not accompanied by a corresponding ROA signal.

Conformational Sensitivity of ROA. In principle, both the Raman and ROA spectra carry information about the conformation. However, due to the limited precision of experiment and simulations, only ROA exhibits recognizable differences. For example, as documented in Figure 5, the all-A-puckering provides quite different spectra than the all-B-puckering. In particular, within 1100−1300 cm^{-1}, many ROA bands are opposite in A and B, which corresponds to the approximately opposite chirality of the five-membered ring in these two forms.

The averaged (over A/B) spectra of conformations differing in the *cis*- and *trans*-amide bonds (cc, tt, Figure 5) are very similar within 200−1100 cm^{-1}. The Boltzmann averaging over all

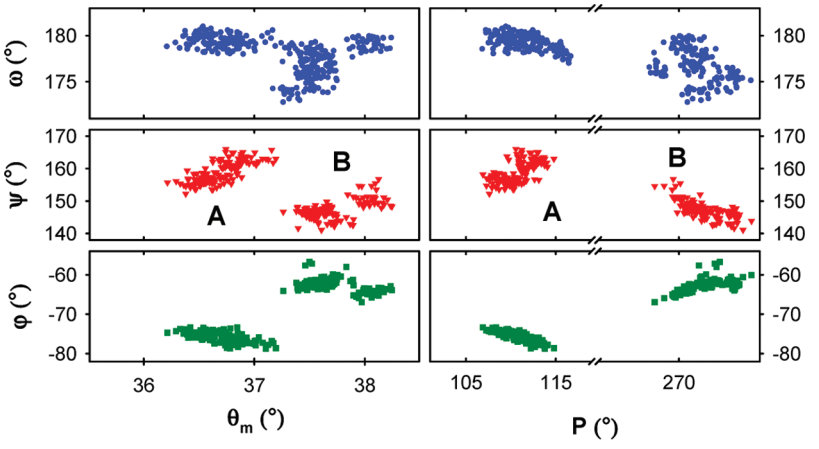

Figure 3. Correlation between the puckering amplitude θ_m and phase P, and main chain torsion angles (cf. Figure 1), as obtained for 64 PPII conformers of $(Pro)_6$ at the B3LYP/CPCM/6-311++G** level.

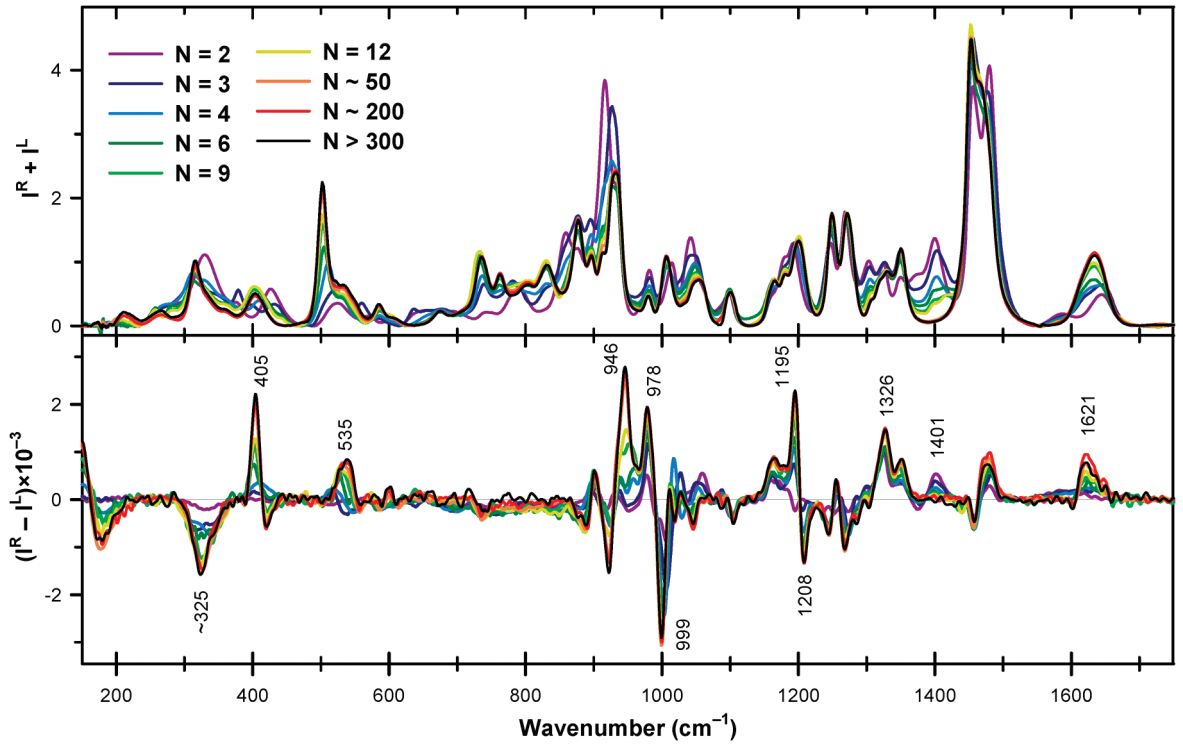

Figure 4. Experimental Raman (top) and ROA (bottom) spectra of the proline oligomers.

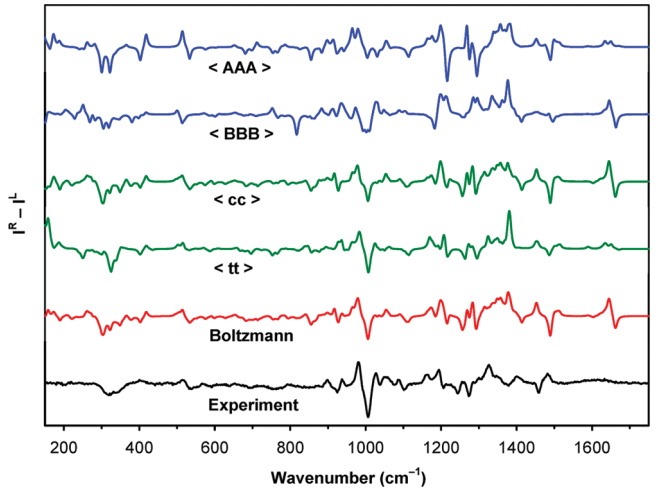

Figure 5. Dependence of the ROA trimer spectra on the conformation. From top to bottom: calculated spectra for the AAA and BBB puckering (*cis*- and *trans*-amide averaged), cc and tt amide structures (puckering averaged), Boltzmann average of all conformations, and the experiment.

conformers is best representing the experiment; if we allow for minor scaling (frequency shift which can be accounted for by the solvent, anharmonic effects, and DFT inaccuracy), we see that most of the ROA bands are reproduced with correct signs.

The large positively biased ROA couplet (~1650 cm^{-1}) of the strongly hydrated NH_2^+ and C=O groups is not seen in experiment, where only a positive plateau remains, which can be explained by the hydrogen bonding and water configuration averaging, only partially involved in the implicit dielectric solvent model.[78,83−85] Larger deviations between the theoretical and experimental frequencies appear also within 1210−1400 cm^{-1}. This region can be affected by anharmonic interactions, presumably present in the C−H bending modes,[77] higher density of vibrational states, and general error of the DFT force field and potential energy surface. Overall, however, the Boltzmann-averaged spectrum clearly reproduces the most prominent experimental ROA features, including the inhomogeneous broadening of spectral bands[86] caused by the multiconformer equilibrium. The corresponding Raman spectra can be found in Figure S3.

ROA Length Dependence. The Boltzmann-averaged spectra faithfully reproduce the observed length dependence. This is documented for the 250−500 cm^{-1} and 825−1050 cm^{-1} wavenumber regions, where the ROA spectra are expanded in Figure 6. Note that the simulation for the longer peptides ($N > 6$) is not possible at the same level, due to the unfeasible computational time and a large number of conformers. Thus, the simulated results for $N = 9$ and 12 in the right upper panel of Figure 6 were obtained by the transfer for the A puckering, and their intensity is somewhat overestimated due to the lack of the averaging.

Nevertheless, we can see that the simulation reproduces not only the spectral pattern, but also the main trends in the ROA spectral dependence on the chain length. For example, the band at ~402 cm^{-1} (experimental frequency is given) is absent for the shortest oligoprolines, but it is well-developed for $N \geq 6$. An intermediate intensity of $(Pro)_4$ is present both in experiment and in simulation. Similarly, the negative intensity around 325 cm^{-1} grows in magnitude with N; however, unlike for the 402 cm^{-1} band, a weak negative signal is present already for the dimer. Within 825−1050 cm^{-1}, the pattern simulated for $N = 6$ resembles more the experiment for $N = 9$ than the hexamer, most probably due to the peptide flexibility only partially accounted for in the modeling. For $N = 9$ and 12, the simulated (transferred)

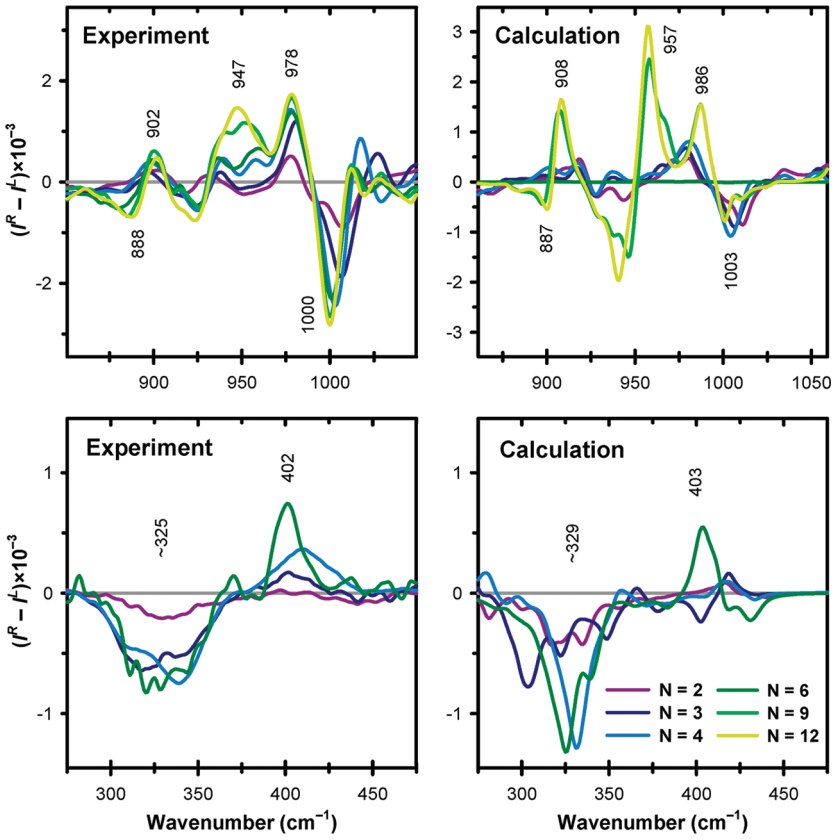

Figure 6. Two spectral regions (up and down): the experimental (left) and simulated (right) ROA spectra for $(Pro)_N$ documenting the length dependence.

results also well reproduce the trends in the spectral shapes, except for the large intensity caused by the limited averaging.

On the basis of the simulations, the Raman and ROA signal and its length-dependence can clearly be related to the structure. For example, the terminal groups with symmetric (1305 cm^{-1}) and asymmetric (1570 cm^{-1}) C═O stretching of the carboxyl group, and NH_2^+ wagging motion at ∼1400 cm^{-1} provide relatively large Raman and ROA signals in the dimer, which, however, quickly recede with the increasing length of the proline chain.

Quite often, ROA signal increase is associated with delocalized, exciton-like vibrations. This can be related to the regularity of the structure as discussed previously for a circular dichroism enhancement.[41] According to our knowledge, this phenomenon was not observed for the Raman and ROA spectra so far. For example, the C═O stretching Raman band (∼1625 cm^{-1}) is significantly enhanced, as the main chain predominantly adopts the trans PPII form. Also some of the ring deformation modes are enhanced in Raman, and some other exhibit higher CID (ROA/Raman) ratio. When the dependence of selected ROA bands on the chain length was simulated by the CCT method for $N = 2, ..., 100$ (Figure 7) we could see that the saturation of the normalized signal is achieved at $N \sim 40$, although the signal continues to grow less steeply also beyond this limit.

The simulation predicts the most favorable intensity enhancement for the regular all-A puckering arrangement in the regular PPII chain (Figure 7). The all-B conformer provides a smaller enhancement, which can be explained by a different coupling leading to different exciton modes.[41] The alternate AB form where the regularity is perturbed most also provides very weak enhancements, again in agreement with the exciton model, as individual oscillators in proline rings may have different frequencies and do not couple strongly in this case.

The simulated development of the Raman and ROA signals with the proline chain length is in good agreement with the observations. We suppose that the proline chain is not so regular as in the simulation, for example, straight segments with $N \sim 50$ are very rare. Because of thermal fluctuations and structural irregularities, we can expect a saturation in experiment for shorter lengths ($N \sim 12-50$), which is in fact observable in Figures 4 and 6. An example of the experimental ROA band progression is given in Figure 8. Here, the relative intensity of the perhaps most distinct 946 cm^{-1} ROA band is plotted in dependence on the chain length. For small N the intensity rises almost linearly, and saturates for the shorter oligomer, with $N \sim 50$. The CID ratio (ROA/Raman) is progressing in the similar way, as the Raman signal is almost constant (cf., Figure 4). As expected, the mode giving the highest intensity predicted by the simulations for the hexamer is delocalized along the peptide chain (top of Figure 8). This is in a perfect agreement with the predicted dependence (Figure 7), but only for the homoconformers (all-A or all-B). We can therefore suppose an occurrence of longer homopuckered sequences in the proline chain.

Theoretical and Experimental Conformer Ratios. We find it remarkable that computed Boltzmann ratios of the conformers can be directly verified by a decomposition of the experimental ROA spectra to the limited number of scaled simulated subspectra representing individual conformer classes. Obviously, decomposition into too many conformers would not be mathematically

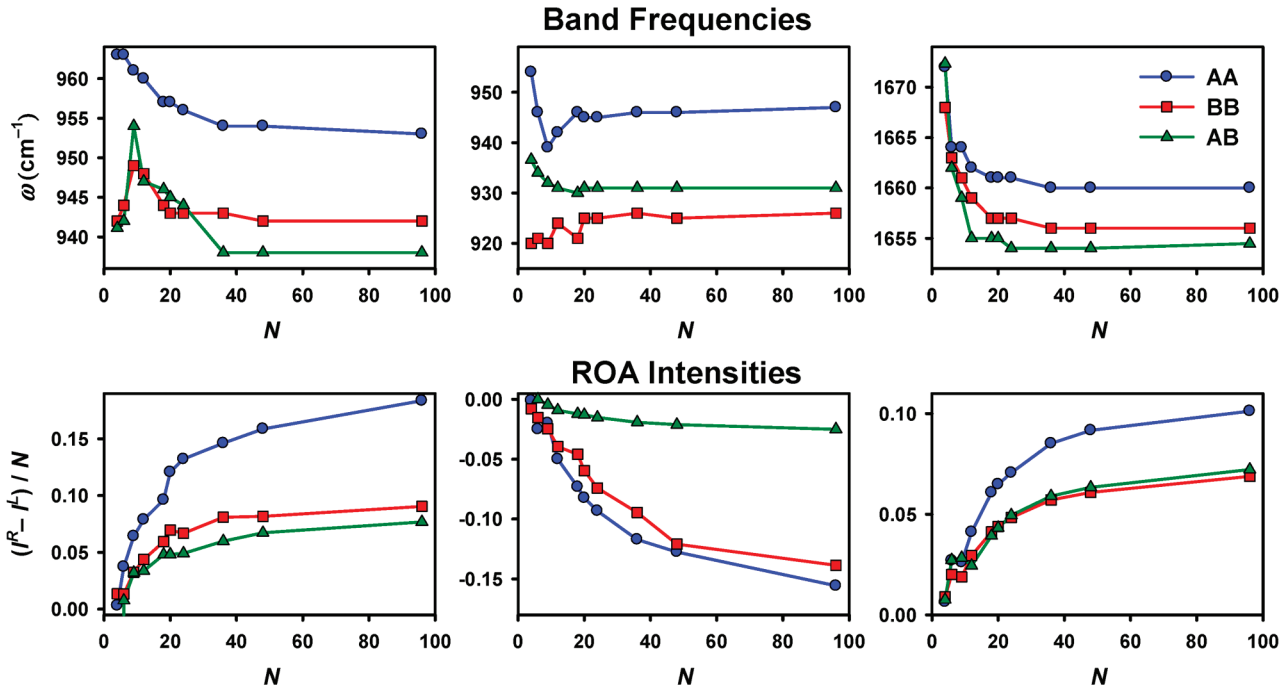

Figure 7. Frequency (top) and ROA intensity (bottom) dependence on the length of the $(Pro)_N$ chain, simulated for three bands and regular PPII all-A ("AA"), all-B ("BB"), and alternate AB puckering patterns.

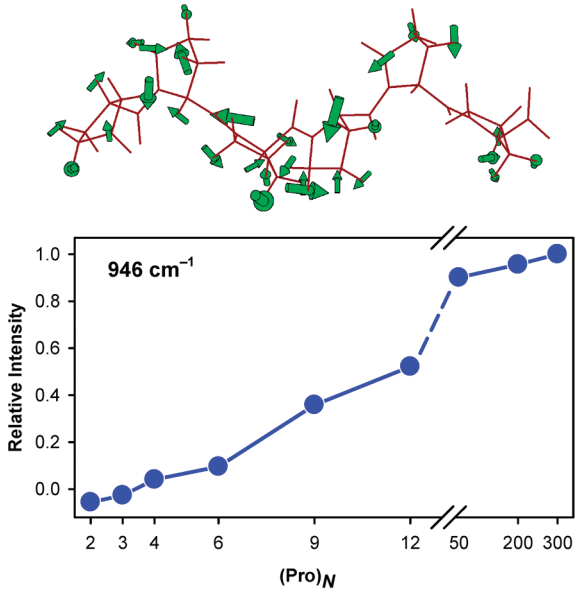

Figure 8. Experimental dependence of the normalized ROA band at 946 cm^{-1} on the $(Pro)_N$ chain length. The most intense vibrational mode of this band as simulated at the B3LYP/6311++G**/CPCM level is displayed above.

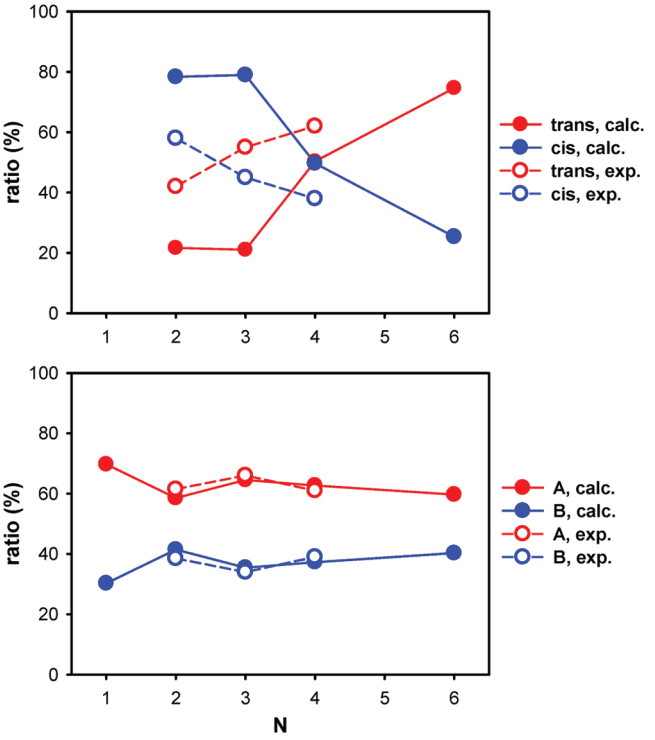

Figure 9. Secondary structure (cis = PPI and trans = PPII) and puckering (A and B) ratios in $(Pro)_N$, computed Boltzmann populations (B3LYP/CPCM/6-311++G**), and percentages obtained from the decomposition of experimental ROA spectra into calculated spectra.

well-defined; however, decompositions into the two or three subspectra provide very encouraging results.

This is documented in Figure 9, where the total cis/trans and A/B content determined by the root-mean-square spectral decomposition[39,52,73] is compared to the Boltzmann weights. The decomposition cannot be done for $N > 4$ due to the huge number of conformers required for the calculations. The puckering A/B ratio of about 60/40 (lower part of Figure 9) is relatively stable over the entire range of the peptide chain lengths, which is consistent with previous computational and X-ray studies,

dx.doi.org/10.1021/jp207706p |J. Phys. Chem. B 2011, 115, 15079–15089

Table 3. Calculated (Boltzmann, B3LYP/CPCM/6311++G) and Experimental Conformer Classes' Ratios (%) in Dimer, Trimer, and Tetramer**

class	calculated	experimental[a]	experimental[b]
Dimer			
prevalent A	36	38	43
prevalent B	16	18	20
equal A, B contents	48	44	37
prevalent cis (PPI)	81	45	58
prevalent trans (PPII)	19	55	42
Trimer			
prevalent A	72	73	66
prevalent B	28	27	34
prevalent cis (PPI)	73	26	27
prevalent trans (PPII)	15	54	37
equal c/t	12	20	36
Tetramer			
prevalent A	52	77	45
prevalent B	15	12	23
equal A, B contents	33	10	32
prevalent cis (PPI)	51	39	38
prevalent trans (PPII)	49	61	62

[a] Algebraic sum of subspectra in a class. [b] Boltzmann-weighted subspectra in a class. For example, the prevalent A subspectrum was Boltzmann averaged over the *cis*- and *trans*-forms.

where in general a 1:1 population is presumed in proteins and peptides.[25,28,29,31,34,35,87−89]

The increasing folding into the *trans*-amide (polyproline II) structure corresponds well to the previous polyproline chain dependence studied by the VCD spectra, which selectively probe the main chain secondary structure.[16,17,56] However, our results also indicate that the PPII folding is gradual, and ratios of pure all-PPII or all-A, and so on, forms are fairly low. The cis/trans ratio (upper part of Figure 9) determined by the energy weighting follows the experimental dependence, although it is consistently larger. We explain this primarily by the error of the PCM solvent correction, which may not well represent the hydrogen bonds stabilizing the secondary structure.[83] Also, as documented in Figure 5, the ROA spectra may not be so sensitive to the cis/trans change as to the A/B puckering difference.

A more detailed summary of the spectral decomposition and calculated Boltzmann weights is given in Table 3, pure conformer species are compared in Figure S4. We can see (Table 3) that the experimental weights somewhat vary according to the decomposition details (the last two columns correspond to decompositions without (algebraic sum) and with Boltzmann weighting within the conformer classes). With the presumably more accurate Boltzmann weighting, the A/B puckering ratios are well reproduced (within a few %), whereas larger deviations occur for the *cis*/*trans*-amide bond ratios.

CONCLUSIONS

We performed a joint computational and Raman/ROA spectroscopic characterization of zwitterionic oligoproline molecules. The quality of the experimental spectra allowed us to follow the dependence of the signal on the number of proline residues in the molecule. The experiment could be well-explained on the basis of calculated relative conformer energies and simulated spectral intensities.

The computation provided insight into the polyproline folding mechanism, interplay between the side chain conformation and polyproline secondary structure, and the most probable puckering patterns. The investigated sequences ($N \sim 2, ..., 6$) fall into the transition state between cis and mixed c/t forms and longer peptides probably dominated by the regular polyproline II structure. The predicted correlations between the main and side chain geometry parameters were in agreement with previous X-ray data.

The ROA spectroscopy proved to be extremely sensitive to the A/B puckering, and slightly less to the *cis*/*trans*-proline amide group conformation. The simulated spectra well explained the observed intensity patterns and the proline chain length dependence. The normal-mode analysis and vibrational assignment revealed that a delocalization in phonon-like vibrations can lead to a significant enhancement of the ROA/Raman intensity ratios, which, in turn, can be used to verify the predicted conformation and regularity of the peptide chain. The study also suggests that the protein folding is a dynamic and gradual process.

ASSOCIATED CONTENT

Supporting Information. Computed relative energies for oligoproline conformers, employing different methods and additional computational details. This material is available free of charge via the Internet at http://pubs.acs.org.

AUTHOR INFORMATION

Corresponding Author
*E-mail: bour@uochb.cas.cz.

ACKNOWLEDGMENT

The work was supported by the Academy of Sciences (M200550902), Grant Agency of the Czech Republic (P208/11/0105), the KONTAKT II MSMT program (LH11033), Norwegian Research Council through a Center of Excellence (179568/V30), by a grant of computer time from the Norwegian Supercomputing Program (Notur).

REFERENCES

(1) Docampo, Z. R.; Pascu, S. I.; Kubik, S.; Otto, S. *J. Am. Chem. Soc.* **2006**, *128*, 11206.
(2) Gibbs, A. C.; Bjorndahl, T. C.; Hodges, R. S.; Wishart, D. S. *J. Am. Chem. Soc.* **2002**, *124*, 1203.
(3) Buděšínský, M.; Šebestík, J.; Bednárová, L.; Baumruk, V.; Šafařík, M.; Bouř, P. *J. Org. Chem.* **2008**, *73*, 1481.
(4) Haque, T. S.; Little, J. C.; Gellman, S. H. *J. Am. Chem. Soc.* **1996**, *118*, 6975.
(5) Rai, R.; Aravinda, S.; Kanagarajadurai, K.; Raghothama, S.; Shamala, N.; Balaram, P. *J. Am. Chem. Soc.* **2006**, *128*, 7916.
(6) Tooke, L.; Duitch, L.; Measey, T. J.; Schweitzer-Stenner, R. *Biopolymers* **2009**, *93*, 451.
(7) Forster, M.; Dyer, M. S.; Persson, M.; Raval, R. *J. Am. Chem. Soc.* **2009**, *131*, 10173.
(8) Kang, Y. K.; Jhon, J. S.; Park, H. S. *J. Phys. Chem. B* **2006**, *110*, 17645.
(9) Song, I. K.; Kang, Y. K. *J. Phys. Chem. B* **2005**, *109*, 16982.

(10) Haasnoot, C. A. G.; DeLeeuw, F. A. A. M.; DeLeeuw, H. P. M.; Altona, C. *Biopolymers* **1981**, *20*, 1211.
(11) Tarakeshwar, P.; Manogaran, S. *J. Mol. Struct.: THEOCHEM* **1996**, *365*, 167.
(12) Sandvoss, L. M.; Carlson, H. A. *J. Am. Chem. Soc.* **2003**, *125*, 15855.
(13) Kakinoki, S.; Hirano, Y.; Oka, M. *Polym. Bull.* **2005**, *53*, 109.
(14) Steinberg, I. Z.; Harrington, W. F.; Berger, A.; Sela, M.; Katchalski, E. *J. Am. Chem. Soc.* **1960**, *82*, 5263.
(15) Stapley, B. J.; Creamer, T. P. *Protein Sci.* **1999**, *8*, 587.
(16) Dukor, R. K.; Keiderling, T. A.; Gut, V. *Int. J. Pept. Protein Res.* **1991**, *38*, 198.
(17) Dukor, R. K.; Keiderling, T. A. *Biopolymers* **1991**, *31*, 1747.
(18) Shi, Z.; Woody, R. W.; Kallenbach, N. R. *Adv. Protein Chem.* **2002**, *62*, 163.
(19) Liu, Z.; Chen, K.; Ng, A.; Shi, Z.; Woody, R. W.; Kallenbach, N. R. *J. Am. Chem. Soc.* **2004**, *126*, 15141.
(20) Blanch, E. W.; Gill, A. C.; Rhie, A. G. O.; Hope, J.; Hecht, L.; Nielsen, K.; Barron, L. D. *J. Mol. Biol.* **2004**, *343*, 467.
(21) Sreerama, N.; Woody, R. W. Circular dichroism of peptides and proteins. In *Circular Dichroism Principles and Applications*; Nakanishi, K., Berova, N., Woody, R. W., Eds.; Wiley-VCH: New York, 2000; p 601.
(22) Engel, J. *Biopolymers* **1966**, *4*, 945.
(23) Zhang, R.; Madalengoitia, J. S. *Tetrahedron Lett.* **1996**, *37*, 6235.
(24) Rothe, M.; Root, H. *Angew. Chem., Int. Ed.* **1976**, *15*, 770.
(25) Kang, Y. K.; Park, H. S. *J. Mol. Struct.: THEOCHEM* **2005**, *718*, 17.
(26) Zhong, H.; Carlson, H. A. *J. Chem. Theory Comput.* **2006**, *2*, 342.
(27) Kang, Y. K. *J. Phys. Chem. B* **2006**, *110*, 21338.
(28) Aliev, A. E.; Courtier-Murias, D. *J. Phys. Chem. B* **2007**, *111*, 14034.
(29) Vitagliano, L.; Berisio, R.; Mastrangelo, A.; Mazzarella, L.; Zagari, A. *Protein Sci.* **2006**, *10*, 2627.
(30) Lee, K. K.; Hahn, S.; Oh, K. I.; Choi, J. S.; Joo, C.; Lee, H.; Han, H.; Cho, M. *J. Phys. Chem. B* **2006**, *110*, 18834.
(31) Kang, Y. K.; Choi, H. Y. *Biophys. Chem.* **2004**, *11*, 135.
(32) Moradi, M.; Babin, V.; Sagui, C.; Roland, C. *Biophys. J.* **2011**, *100*, 1083.
(33) Pecul, M.; Ruud, K.; Rizzo, A.; Helgaker, T. *J. Phys. Chem. A* **2004**, *108*, 4269.
(34) Kapitán, J.; Baumruk, V.; Kopecký, V., Jr.; Pohl, R.; Bouř, P. *J. Am. Chem. Soc.* **2006**, *128*, 13451.
(35) Kapitán, J.; Baumruk, V.; Kopecký, V., Jr.; Bouř, P. *J. Am. Chem. Soc.* **2006**, *128*, 2438.
(36) Moradi, M.; Babin, V.; Roland, C.; Sagui, C. *J. Chem. Phys.* **2010**, *133*, 125104.
(37) Moradi, M.; Babin, V.; Roland, C.; Darden, T. A.; Sagui, C. *Proc. Natl. Acad. Sci. U.S.A.* **2009**, *106*, 20746.
(38) Moradi, M.; Lee, J.; Babin, V.; Roland, C.; Sagui, C. *Int. J. Quantum Chem.* **2010**, *110*, 2865.
(39) Buděšínský, M.; Daněček, P.; Bednárová, L.; Kapitán, J.; Baumruk, V.; Bouř, P. *J. Phys. Chem. A* **2008**, *112*, 8633.
(40) Profant, V.; Šafařík, M.; Bouř, P.; Baumruk, V. *Spectroscopy* **2010**, *24*, 213.
(41) Andrushchenko, V.; Bouř, P. *J. Comput. Chem.* **2008**, *29*, 2693.
(42) Šebestík, J.; Bouř, P. *J. Phys. Chem. Lett.* **2011**, *2*, 498.
(43) Polavarapu, P. L. *Angew. Chem., Int. Ed.* **2002**, *41*, 4544.
(44) Haesler, J.; Schindelholz, I.; Riguet, E.; Bochet, C. G.; Hug, W. *Nature* **2007**, *446*, 526.
(45) Jalkanen, K. J.; Nieminen, R. M.; Knapp-Mohammady, M.; Suhai, S. *Int. J. Quantum Chem.* **2003**, *92*, 239.
(46) Hudecová, J.; Kapitán, J.; Baumruk, V.; Hammer, R. P.; Keiderling, T. A.; Bouř, P. *J. Phys. Chem. A* **2010**, *114*, 7642.
(47) Barron, L. D.; Blanch, E. W.; Hecht, L. *Adv. Protein Chem.* **2002**, *62*, 51.
(48) McColl, I. H.; Blanch, E. W.; Hecht, L.; Barron, L. D. *J. Am. Chem. Soc.* **2004**, *126*, 8181.
(49) Abdali, S.; Jalkanen, K. J.; Cao, X.; Nafie, L. A.; Bohr, H. *Phys. Chem. Chem. Phys.* **2004**, *6*, 2434.
(50) Barron, L. D.; Blanch, E. W.; McColl, I. H.; Syme, C. D.; Hecht, L.; Nielsen, K. *Spectrosc.: Intl. J.* **2003**, *17*, 101.
(51) Blanch, E. W.; McColl, I. H.; Hecht, L.; Nielsen, K.; Barron, L. D. *Vib. Spectrosc.* **2004**, *35*, 87.
(52) Yamamoto, S.; Straka, M.; Watarai, H.; Bouř, P. *Phys. Chem. Chem. Phys.* **2010**, *12*, 11021.
(53) Hahn, S.; Lee, H.; Cho, M. *J. Chem. Phys.* **2004**, *121*, 1849.
(54) Ahmed, Z.; Myshakina, N. S.; Asher, S. A. *J. Phys. Chem. B* **2009**, *113*, 11252.
(55) McColl, I. H.; Blanch, E. W.; Hecht, L.; Kallenbach, N. R.; Barron, L. D. *J. Am. Chem. Soc.* **2004**, *126*, 5076.
(56) Dukor, R. K.; Keiderling, T. A. *Biospectroscopy* **1996**, *2*, 83.
(57) Cheeseman, J. R. *Calculation of Molecular Chiroptical Properties using Density Functional Theory*. In *CD 2007*; University of Groningen: Groningen, 2007; p inv 3.
(58) Ruud, K.; Thorvaldsen, J. *Chirality* **2009**, *21*, E54.
(59) Liegeois, V.; Ruud, K.; Champagne, B. *J. Chem. Phys.* **2007**, *127*, 204105.
(60) Ruud, K.; Helgaker, T.; Bouř, P. *J. Phys. Chem. A* **2002**, *106*, 7448.
(61) Bouř, P.; Sopková, J.; Bednárová, L.; Maloň, P.; Keiderling, T. A. *J. Comput. Chem.* **1997**, *18*, 646.
(62) Yamamoto, S.; Bouř, P. *Collect. Czech. Chem. Commun.* **2011**, *76*, 567.
(63) Bieler, N. S.; Haag, M. P.; Jacob, C. R.; Reiher, M. *J. Chem. Theory Comput.* **2011**, *7*, 1867.
(64) Profant, V.; Bouř, P.; Baumruk, V. Folding studies of proline oligomers by the Raman optical activity. In *CD 2011*; Diamond Light Source: Oxford, 2011; p. 49.
(65) Hanzlíková, J.; Praus, P.; Baumruk, V. *J. Mol. Struct.* **1999**, *480−481*, 431.
(66) Momany, F. A.; McGuire, R. F.; Burgess, A. W.; Scheraga, H. A. *J. Phys. Chem.* **1975**, *79*, 2361.
(67) Altona, C.; Sundaralingam, M. *J. Am. Chem. Soc.* **1972**, *94*, 8205.
(68) Frisch, M. J.; Trucks, G. W.; Schlegel, H. B.; Scuseria, G. E.; Robb, M. A.; Cheeseman, J. R.; Scalmani, G.; Barone, V.; Mennucci, B.; Petersson, G. A.; Nakatsuji, H.; Caricato, M.; Li, X.; Hratchian, H. P.; Izmaylov, A. F.; Bloino, J.; Zheng, G.; Sonnenberg, J. L.; Hada, M.; Ehara, M.; Toyota, K.; Fukuda, R.; Hasegawa, J.; Ishida, M.; Nakajima, T.; Honda, Y.; Kitao, O.; Nakai, H.; Vreven, T.; Montgomery, J., J. A.; Peralta, J. E.; Ogliaro, F.; Bearpark, M.; Heyd, J. J.; Brothers, E.; Kudin, K. N.; Staroverov, V. N.; Kobayashi, R.; Normand, J.; Raghavachari, K.; Rendell, A.; Burant, J. C.; Iyengar, S. S.; Tomasi, J.; Cossi, M.; Rega, N.; Millam, J. M.; Klene, M.; Knox, J. E.; Cross, J. B.; Bakken, V.; Adamo, C.; Jaramillo, J.; Gomperts, R.; Stratmann, R. E.; Yazyev, O.; Austin, A. J.; Cammi, R.; Pomelli, C.; Ochterski, J. W.; Martin, R. L.; Morokuma, K.; Zakrzewski, V. G.; Voth, G. A.; Salvador, P.; Dannenberg, J. J.; Dapprich, S.; Daniels, A. D.; Farkas, O.; Foresman, J. B.; Ortiz, J. V.; Cioslowski, J.; Fox, D. J. *Gaussian 09*, Revision A.02; Gaussian, Inc.: Wallingford, CT, 2009.
(69) Becke, A. D. *J. Chem. Phys.* **1993**, *98*, 5648.
(70) Klamt, A.; Jonas, V.; Burger, T.; Lohrentz, J. C. W. *J. Phys. Chem. A* **1998**, *102*, 5074.
(71) Rappe, A. K.; Casewit, C. J.; Colwell, K. S.; Goddard, W. A., III; Skiff, W. M. *J. Am. Chem. Soc.* **1992**, *114*, 10024.
(72) Grimme, S. *J. Comput. Chem.* **2006**, *27*, 1787.
(73) Yamamoto, S.; Watarai, H.; Bouř, P. *ChemPhysChem* **2011**, *12*, 1509.
(74) Parchaňský, V.; Matějka, P.; Dolenský, B.; Havlík, M.; Bouř, P. *J. Mol. Struct.* **2009**, *934*, 117.
(75) Kang, Y. K.; Byun, B. J. *J. Comput. Chem.* **2010**, *31*, 2915.
(76) Bouř, P.; Kapitán, J.; Baumruk, V. *J. Phys. Chem. A* **2001**, *105*, 6362.
(77) Daněček, P.; Kapitán, J.; Baumruk, V.; Bednárová, L.; Kopecký, V., Jr.; Bouř, P. *J. Chem. Phys.* **2007**, *126*, 224513.
(78) Hopmann, K. H.; Ruud, K.; Pecul, M.; Kudelski, A.; Dračínský, M.; Bouř, P. *J. Phys. Chem. B* **2011**, *115*, 4128.
(79) Grathwohl, C.; Wüthrich, K. *Biopolymers* **1976**, *15*, 2026.
(80) Deslauriers, R.; Smith, I. C. P. *J. Biol. Chem.* **1974**, *249*, 7006.

(81) Creighton, T. E. *Proteins: Structures and Molecular Properties*, 2nd ed.; W. H. Freeman and Co.: New York, 1993.
(82) Andrushchenko, V.; Matějka, P.; Anderson, D. T.; Kaminský, J.; Horníček, J.; Paulson, L. O.; Bouř, P. *J. Phys. Chem. A* **2009**, *113*, 9727.
(83) Bouř, P.; Michalík, D.; Kapitán, J. *J. Chem. Phys.* **2005**, *122*, 144501.
(84) Jalkanen, K. J.; Degtyarenko, I. M.; Nieminen, R. M.; Cao, X.; Nafie, L. A. *Theor. Chem. Acc.* **2008**, *119*, 191.
(85) Knapp-Mohammady, M.; Jalkanen, K. J.; Nardi, F.; Wade, R. C.; Suhai, S. *Chem. Phys.* **1999**, *240*, 63.
(86) Kapitán, J.; Baumruk, V.; Kopecký, V., Jr.; Bouř, P. *J. Phys. Chem. A* **2006**, *110*, 4689.
(87) Sarkar, K.; Young, P. E.; Torchia, D. A. *J. Am. Chem. Soc.* **1986**, *108*, 6459.
(88) Kayushina, R. L.; Vainshtein, B. K. *Crystallogr. Rep.* **1965**, *10*, 833.
(89) Kang, Y. K. *J. Phys. Chem. B* **2004**, *108*, 5463.